ACS Catalysis

Research Article

pubs.acs.org/acscatalysis

Nitrogen-Functionalized Ordered Mesoporous Carbons as Multifunctional Supports of Ultrasmall Pd Nanoparticles for Hydrogenation of Phenol

Zelong Li,[†,§] Jianhua Liu,[†] Chungu Xia,*[,†] and Fuwei Li*[,†,‡]

[†]State Key Laboratory for Oxo Synthesis and Selective Oxidation, Lanzhou Institute of Chemical Physics, Chinese Academy of Sciences, Lanzhou, Gansu 730000, P. R. China

[‡]Suzhou Institute of Nano-Tech and Nano-Bionics, Chinese Academy of Sciences, Suzhou, Jiangsu 215123, P. R. China

[§]University of the Chinese Academy of Sciences, Beijing, P. R. China

Supporting Information

ABSTRACT: N-functionalized ordered mesoporous carbons could be readily obtained by post-synthesis treatment with nitrogen containing molecules to achieve materials with a nitrogen loading as high as 8.6 wt % and well preserved mesopore structure. Using NH_3 as nitrogen source dramatically increased the Brunauer–Emmett–Teller (BET) surface area and pore volume of the resultant hybrid material; however, N-doping with melamine as a source resulted in the contrary results. The N-doped carbons were used as supports to immobilize small-sized Pd nanoparticles (PdNPs), which provided a unique platform to investigate the influence of metal nanoparticle size, mesostructural properties, and N-functionalized supports on the selective hydrogenation of phenol to cyclohexanone, an important intermediate in the production of nylon 6 and nylon 66 in the chemical industry. The catalyst with ultrasmall (about 1.2 nm) PdNPs gave the best reaction activity and selectivity under mild conditions. In addition, the present multifunctional catalyst demonstrated excellent catalytic stability and could be used 6 times without loss of product yields. This outstanding catalytic performance could be attributed to the synergetic effects of mesoporous structure, N-functionalized supports, and the stabilized ultrasmall PdNPs. This work might open new avenues for the development of functionalized catalysts with supported ultrasmall metal nanoparticles and hybrid porous support as well as their clean catalyses.

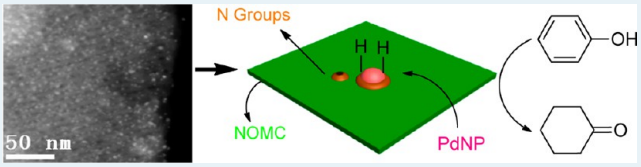

KEYWORDS: *N-doped ordered mesoporous carbon, hydrogenation, ultrasmall Pd nanoparticles, heterogeneous catalysis*

1. INTRODUCTION

The downscaling and control of supported metal nanoparticle (NP) sizes have become an important topic for the development of new and efficient heterogeneous catalytic materials.[1−4] Downsizing the NPs to a few nanometers or even subnanometers can dramatically increase their ratio of surface to bulk atoms, which may influence the total energy and fundamental properties of NPs, and thus can affect their catalytic performance in the reactions. However, a major challenge for using supported ultrasmall metal NP catalysts is to prevent the leaching of metal NPs from the supports and the growth of metal NPs during reactions, especially under harsh conditions.[5−8] Hence maintaining the stability of the NP catalyst is crucial, and building interactions between the small-sized metal NPs and functionalized supports (such as nitrogen-doped carbons) is one of the most important solutions to achieve such stabilization and even activation, since a certain degree of chemical engagement (such as coordination and electron transfer) between them can reduce the mobility of the catalytic metals and thus prevent them from aggregating or sintering.[9] Additionally, compared with amorphous supports, the ordered mesoporous supports with high surface area and large pore volume can favor mass transfer and show the confinement effect to prevent the metal NPs' growth as well, which are all beneficial to efficient catalysis.[10−12] Therefore, combining the confinement effect and hybrid doping of the ordered mesoporous supports, the N-functionalized (e.g., nitrogen) mesoporous nanomaterial can be an ideal alternative catalyst support for the immobilization and stabilization of ultrasmall metal NPs.

Recently, nanostructured mesoporous carbon nitrides were widely prepared by thermal polycondensation of different monomers through hard-template synthesis, and these ordered N-doped carbon matrixes have been successfully used as supports to synthesize supported NP catalysts for efficient hydrogenation,[13−16] oxidation,[17] and coupling reaction,[18] because the N-doping could not only change the physicochemical and electronic properties of the support, but also serve as basic or coordination sites to stabilize the small metal NPs or activate some special substrate (such as phenol in its hydrogenation).[19] Besides the hard-templating approach, the incorporation of nitrogen into the carbons can be more easily

Received: July 4, 2013
Revised: September 8, 2013
Published: September 16, 2013

achieved by a postprocess with ammonia or melamine as the nitrogen source.[20−23] Moreover, the post-synthesis methodology can realize surface incorporation with variable nitrogen content. As far as we know, few excellent applications of N-doped ordered mesoporous carbon (OMC) as catalytic support have emerged and therefore it is highly desirable to synthesize the mesoporous analogues and their corresponding supported small-sized NPs catalysts.

As part of our continuing interest in the development of supported metal NPs on N-doped carbons,[24] we herein report the incorporation of N-hybrids into FDU-type OMC materials with NH_3 and melamine, yielding N-incorporated OMC (NOMC) supports with well maintained high surface area and mesostructure (Scheme 1). The resultant carbon supports

Scheme 1. Illustration of the Route to Synthesize PdNPs Supported on the NOMCs

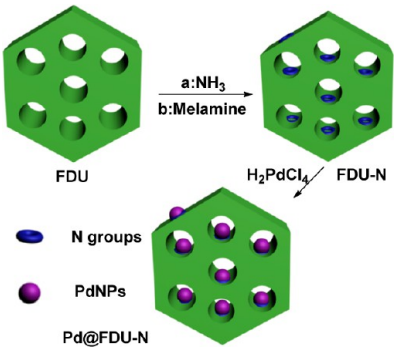

can be ideal catalytic supports to homogeneously immobilize and stabilize ultrasmall Pd nanoparticles (PdNPs), which demonstrate high catalytic activity and selectivity in the hydrogenation of phenol to cyclohexanone under atmospheric hydrogen pressure. Remarkably, the hybrid solid catalysts can be used for six times in the liquid reaction without loss of its product yields.

2. RESULTS AND DISCUSSION

The preparation of the N-doped OMC supports was initially conducted by heat treatment of commercially available FDU-type OMC materials (two different FDU-15 with 3 or 5 nm pore size were named as FDU^3 and FDU^5, respectively) under flowing NH_3 atmosphere, and the obtained NOMC materials were denoted as $FDU^3{-}N^H$ and $FDU^5{-}N^H$ based on different supports. For comparison, another N-functionalized carbon support ($FDU^3{-}N^C$) was also prepared through a simple wet-impregnation of melamine into the mesopore channels of FDU^3 and following carbonization at 700 °C for 2 h. Subsequently, the resultant $FDU^3{-}N^H$, $FDU^5{-}N^H$, and $FDU^3{-}N^C$ were separately utilized as supports to immobilize the PdNPs by the impregnation method to give corresponding $Pd^X@FDU^3{-}N^H$, $Pd^X@FDU^5{-}N^H$, and $Pd^X@FDU^3{-}N^C$ catalysts, wherein X represented the Pd loading percent.

Figure 1 shows the N_2 sorption isotherms and Barrett−Joyner−Halenda (BJH) mesopore size distribution plots of FDU^3, FDU^5, $FDU^3{-}N^H$, $FDU^5{-}N^H$, $Pd^X@FDU^3{-}N^H$, and $Pd^X@FDU^5{-}N^H$. Their corresponding pore character, Brunauer−Emmett−Teller (BET) surface area, and pore volume are summarized in Table 1. All samples show type-IV curves with sharp capillary condensation step and H2-type hysteresis loop, indicative of the uniform pore size distributions of the

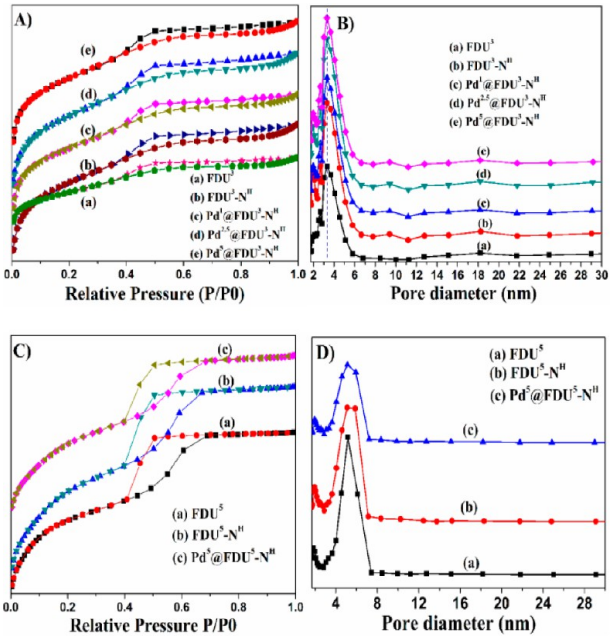

Figure 1. N_2 sorption isotherms (A and C) and BJH mesopore size distribution plots (B and D) of FDU^3, $FDU^3{-}N^H$, $Pd^X@FDU^3{-}N^H$ (A and B), FDU^5, $FDU^5{-}N^H$, $Pd^5@FDU^5{-}N^H$ (C and D).

Table 1. Physicochemical Properties and the N and O Contents of the Mesoporous Nanocomposites

sample	S_{BET} ($m^2\ g^{-1}$)	vol ($m^3\ g^{-1}$)	N wt %[a]
FDU^3	692	0.42	-[b]
$FDU^3{-}N^H$	1100	0.66	8.6
$Pd^1@FDU^3{-}N^H$	1082	0.65	-
$Pd^{2.5}@FDU^3{-}N^H$	1022	0.62	-
$Pd^5@FDU^3{-}N^H$	1006	0.58	-
FDU^5	1247	0.96	-
$FDU^5{-}N^H$	1736	1.26	8.3
$Pd^5@FDU^5{-}N^H$	1487	1.05	-
$FDU^3{-}N^C$	634	0.38	7.8
$Pd^5@FDU^3{-}N^C$	608	0.35	-

[a]Data from the EA. [b]"-" means the data is not detected.

mesopores before and after N-incorporation with NH_3 (Figure 1A). The pore size distributions of N-doped FDU and their supported PdNPs hybrid catalysts are close to their mother nonacomposites (Figure 1B and 1D), both BET surface area and pore volume of $FDU^3{-}N^H$ and $FDU^5{-}N^H$ increase dramatically after the treatment of NH_3 at 700 °C (Table 1), and their S_{BET} values (1100 $m^2\ g^{-1}$ for $FDU^3{-}N^H$ and 1736 $m^2\ g^{-1}$ for $FDU^5{-}N^H$) are much higher than that of the reported NOMCs produced via hard-templating synthesis by using CCl_4/diamine (around 714 $m^2\ g^{-1}$)[25] or cyanamide (179 $m^2\ g^{-1}$)[19] as polymerization substrates. These changes could be attributed to such N-doping reaction nature by use of NH_3 as nitrogen source that proceeded via decomposition of ammonia at high temperature into radicals such as $\bullet NH_2$, $\bullet NH$, and $\bullet H$, which could etch carbon fragment, and these reactions could result in the porosity increase.[22,26−28] The specific surface area and pore volumes of the $Pd^X@FDU{-}N^H$ only decrease slightly after the supporting of the PdNPs and decrease slightly further with the increase of Pd loading (Table 1). Compared with FDU, there is only slight change on the mesoporous size of the $FDU{-}N^H$ and $Pd^X@FDU{-}N^H$, suggesting that the ordered

dx.doi.org/10.1021/cs400506q | ACS Catal. 2013, 3, 2440−2448

mesostructure is still well-preserved after etching by NH_3 and immobilization of PdNPs, and the mesostructure of Pd^X@FDU-N^H and Pd^5@FDU-N^H are not blocked by PdNPs. This phenomenon also corresponds to their following small-angle X-ray diffraction (SAXRD) characterization (Figure 2). It was

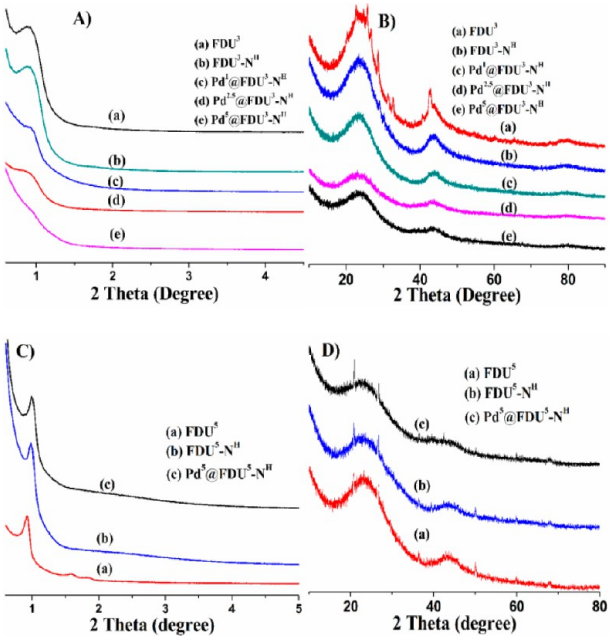

Figure 2. SAXRD (A and C) and WAXRD (B and D) patterns of FDU^3, FDU^3–N^H, Pd^X@FDU^3–N^H (A and B), FDU^5, FDU^5–N^H, Pd^5@FDU^5–N^H (C and D).

worth noting that the ordered mesopore structure was favorable for facilitating mass transfer, and the large enough surface area could allow more contacts between the catalytic active sites and substrates, which are key points for an excellent catalyst.

As presented in Figure 2A and 2C, the SAXRD pattern of FDU^3 shows one resolved peak, which is indexed as the 10 planes of a 2D hexagonal mesostructure with space group *p6m*, and the SAXRD pattern of FDU^5 presents three resolved diffraction peaks that can be assigned to the 10, 11, and 20 diffractions of an ordered 2D hexagonal *p6m* mesostructure. After heat treatment under NH_3, FDU^3–N^H, Pd^X@FDU^3–N^H (X = 1, 2.5, 5), FDU^5–N^H and Pd^5@FDU^5–N^H all show resolved diffraction peaks of hexagonal *p6m* mesostructure (Figure 2). The small decrease in the diffraction intensity in the samples after etching by NH_3 and immobilizing PdNPs indicates that the ordered mesostructures are slightly degenerated. Wide-angle XRD (WAXRD) patterns show that all nanocomposites possess graphitic carbon walls and show high-intensity 002 and 100 diffractions belonging to graphitic carbon. The patterns of Pd^1@FDU^3–N^H, $Pd^{2.5}$@FDU^3–N^H, Pd^5@FDU^3–N^H, and Pd^5@FDU^5–N^H only show 002 and 100 diffractions, and the characteristic diffraction peaks of the Pd are not observed at all. Although the Pd loading content for Pd^5@FDU^3–N^H and Pd^5@FDU^5–N^H is as high as 5 wt %, the PdNPs are still not detected by XRD, which possibly indicates that the supported PdNPs have ultrasmall particle sizes and are homogeneously dispersed on the surface of the N-doped OMC matrix.

Transmission electron microscopy (TEM) was used to examine the structure of the N-incorporated FDU^3–N^H and FDU^5–N^H (Figure 3). The TEM images show that these two samples have high degree of periodicity viewed from the [110]

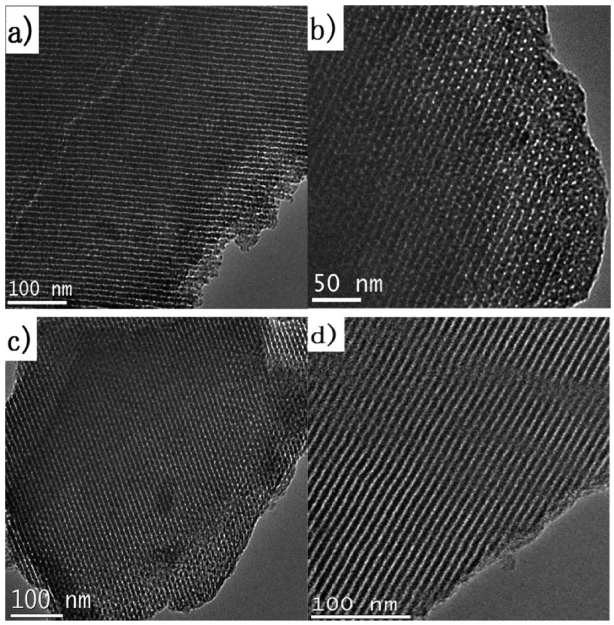

Figure 3. TEM images of (a) FDU^3, (b) FDU^3–N^H, (c) FDU^5, (d) FDU^5–N^H.

direction, and this phenomenon also confirms that these N-doped OMCs still keep a 2D hexagonal mesostructure. Elemental analyses (EA) measurements reveal that the nitrogen content of FDU^3–N^H and FDU^5–N^H can be as high as 8.6 wt % and 8.3 wt % (Table 1), respectively. The X-ray photoelectron spectroscopy (XPS) spectra of the NOMCs show strong signals from carbon, nitrogen, and oxygen elements. The surface nitrogen contents measured from XPS data for FDU^3–N^H and FDU^5–N^H are about 7.7 and 7.5 wt %, respectively, which are all close to their corresponding EA results, implying that the nitrogen element is distributed homogeneously in the framework of OMCs. The N1s XPS peaks of FDU^3–N^H and FDU^5–N^H can be well fitted to two peaks (Figure 4), the lower energy peak near 398.5 eV is

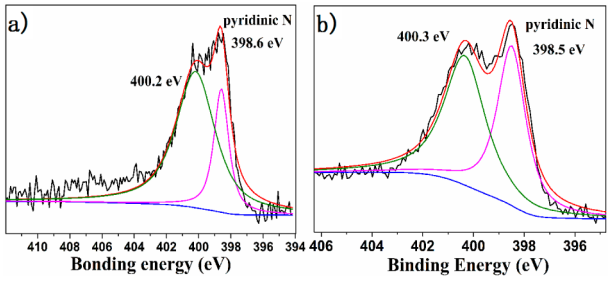

Figure 4. XPS N1s spectra of NOMC: (a) FDU^3–N^H, (b) FDU^5–N^H.

assigned to pyridinic nitrogen, and the peak centered at about 400.2 eV is attributed to pyrrolic-type nitrogen.[29−32] It is reported that the radicals generated from NH_3 at high temperature can replace oxygen-containing species on the carbon to form nitrogen-containing groups and thereby realize the N-incorporation.[22,26] On the other hand, the surface oxygen contents from XPS results also reveal obvious decreases after the NH_3 treatment.

dx.doi.org/10.1021/cs400506q | ACS Catal. 2013, 3, 2440−2448

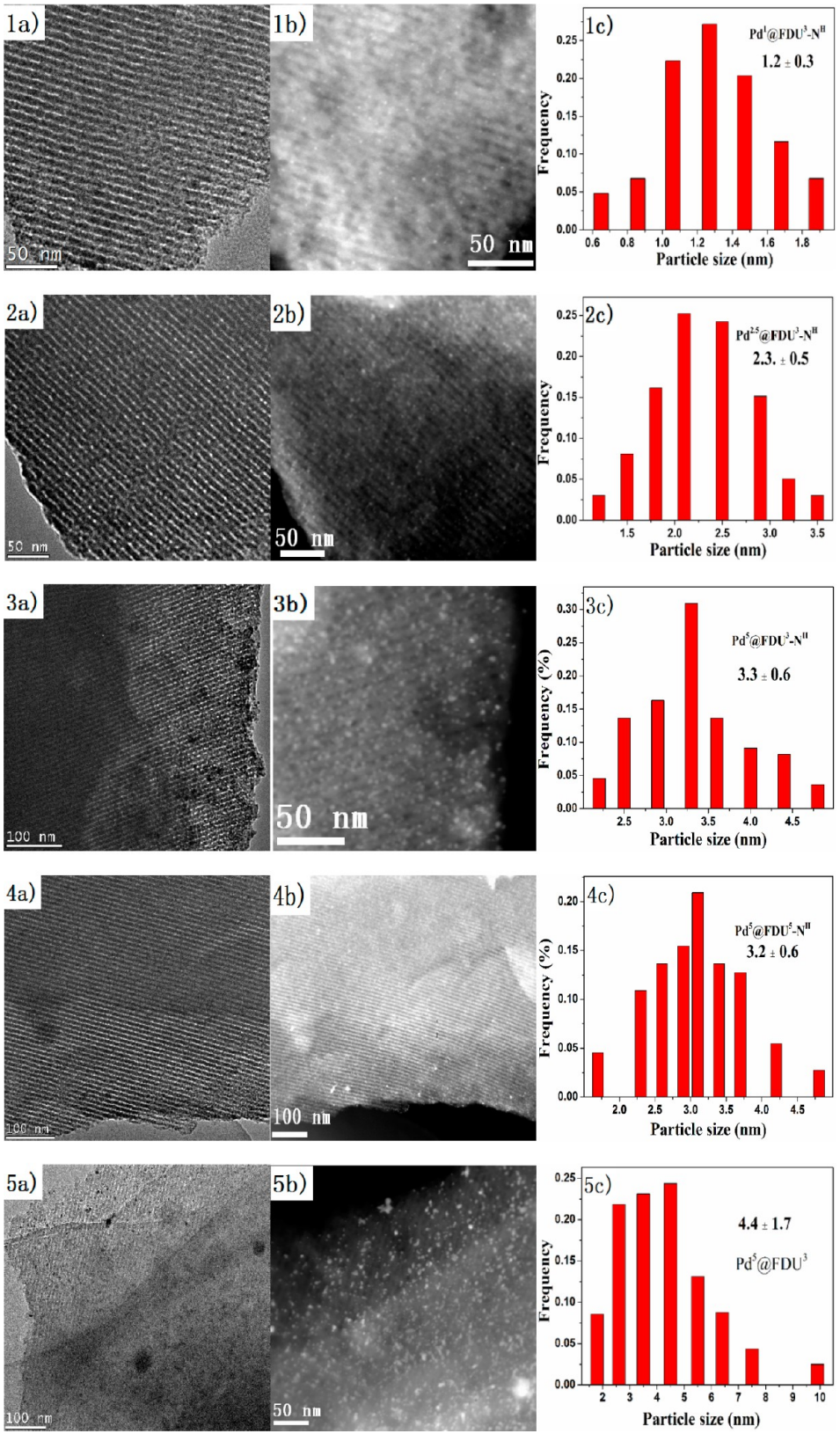

Figure 5. TEM, HAADF-STEM and distribution of particle size images of (1a, 1b, and 1c) $Pd^{1}@FDU^{3}-N^{H}$, (2a, 2b, and 2c) $Pd^{2.5}@FDU^{3}-N^{H}$, (3a, 3b, and 3c) $Pd^{5}@FDU^{3}-N^{H}$, (4a, 4b, and 4c) $Pd^{5}@FDU^{5}-N^{H}$, (5a, 5b, and 5c) $Pd^{5}@FDU^{3}$.

Based on the above observations, the present $FDU^{3}-N^{H}$ and $FDU^{5}-N^{H}$ with high nitrogen content and well maintained mesostructure could possibly be interesting supports for the immobilization of small-sized PdNPs. Initially, TEM is used to test the morphology and distribution of the supported PdNPs on $Pd^{X}@FDU^{3}-N^{H}$ (X = 1, 2.5, 5) and $Pd^{5}@FDU^{5}-N^{H}$; surprisingly, no PdNPs are observed obviously on the surface of these hybrid materials (1a to 4a of Figure 5), which is possibly

dx.doi.org/10.1021/cs400506q | ACS Catal. 2013, 3, 2440−2448

because the untrasmall PdNPs are mainly loaded into the channels of the mesoporous carbons. Their high-angle annular dark-field scanning TEM (HAADF-STEM) images show that the majority of the ultrasmall PdNPs look like white dots and are homogeneously dispersed along the heterogeneous surface of the OMC pores (1b to 4b of Figure 5). All the PdNPs are uniform in size and shape; no agglomeration is observed in the HAADF-STEM images. It is also clearly to see that mesochannels are linearly arranged in regular intervals, indicating that the N-doped ordered mesoporous structure is much stabler for the immobilization of metal NPs. The particle size distributions of the PdNPs for Pd^{1}@FDU^{3}–N^{H}, $Pd^{2.5}$@FDU^{3}–N^{H}, Pd^{5}@FDU^{3}–N^{H}, and Pd^{5}@FDU^{5}–N^{H} are 1.2 ± 0.3, 2.3 ± 0.5, 3.3 ± 0.6, and 3.2 ± 0.6 nm (1c to 4c of Figure 5), respectively. The size of the PdNPs formed on the external surface of the support is slightly larger than that of the PdNPs formed inside the mesochannels for Pd^{X}@FDU^{3}–N^{H} and Pd^{5}@FDU^{5}–N^{H}, which can be attributed to the "confinement effect" of the ordered mesoporous structure to prevent the growth of PdNPs. Moreover, these PdNPs on the external surface are also well-dispersed without aggregation observed because of the stabilization by the incorporated N-hybrids. Interestingly, although the mesopore size of FDU^{5}–N^{H} (5.1 nm) is larger than that of FDU^{3}–N^{H} (3.3 nm), the particle size distribution of their supported PdNPs is quite consistent with each other, possibly indicating that the inbuilt N species on the carbon supports play a key role in preventing the uncontrollable growth of the PdNPs and stabilizing the formed PdNPs effectively. Moreover, the elemental mapping images of a representative Pd^{5}@FDU^{3}–N^{H} also confirm that the nitrogen and Pd atoms are all homogeneously dispersed in the materials (Figure 6).

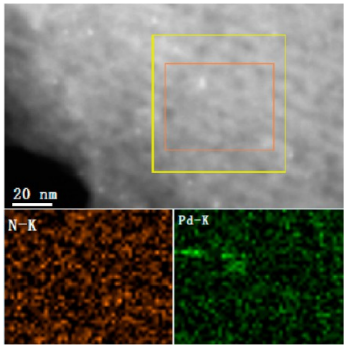

Figure 6. HAADF-STEM images of Pd^{5}@FDU^{3}–N^{H} and corresponding elemental mapping images of N and Pd.

To further clarify the stabilizing role of the N-doped functionalities, original FDU^{3} without N-doping is also utilized as a support to prepare corresponding supported PdNP catalytic material (Pd^{5}@FDU^{3}), as revealed in its TEM and HAADF-STEM images (5a and 5b of Figure 5), most of the PdNPs are distributed on the external surface of the OMC but not inside the channels. Compared with its N-doped analogues, Pd^{5}@FDU^{3}–N^{H}, the particle size distribution of Pd^{5}@FDU^{3} (4.4 ± 1.7 nm) is larger than that of Pd^{5}@FDU^{3}–N^{H} (3.3 ± 0.6 nm) and the PdNPs aggregation of Pd^{5}@FDU^{3} is also observed. These obvious differences reveal that the nitrogen-contained groups can be a key factor in preventing the aggregation of PdNPs and stabilizing the formed PdNPs mainly inside the mesoporous channels and on the surface of OMC as well.

The Pd XPS spectra of Pd^{X}@FDU^{3}–N^{H}, Pd^{5}@FDU^{5}–N^{H}, and Pd^{5}@FDU^{3} present a doublet corresponding to Pd $3d_{5/2}$ and $3d_{3/2}$ (Supporting Information, Figure S1). The Pd $3d_{5/2}$ peak at 335.6 eV is attributed to Pd^{0} (metallic palladium), while the Pd $3d_{5/2}$ peak at 337.5 eV is related to Pd^{2+} (palladium oxide).[27] According to the XPS data of the Pd^{1}@FDU^{3}–N^{H}, $Pd^{2.5}$@FDU^{3}–N^{H}, Pd^{5}@FDU^{3}–N^{H}, and Pd^{5}@FDU^{5}–N^{H}, Pd^{0} is formed as the major phase (roughly >70%) on the surface of the catalysts.

As a comparison with FDU^{3}–N^{H} and its supported PdNPs, N-incorporation of FDU^{3} using melamine as nitrogen source was also conducted to produce FDU^{3}–N^{C}, which was further utilized as a support to synthesize PdNPs supported Pd@FDU^{3}–N^{C}. As shown in their N_2 sorption isotherms and the BJH mesopore size distribution plots (Figure 7), their

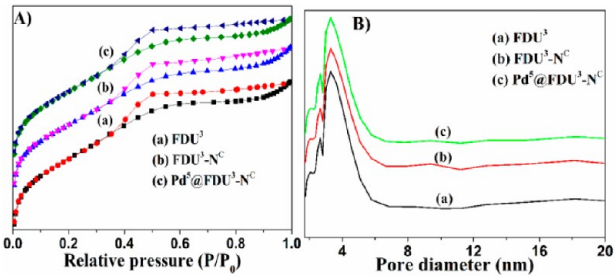

Figure 7. N_2 sorption isotherms (A) and BJH mesopore size distribution plots (B) of FDU^{3}, FDU^{3}–N^{C}, Pd^{5}@FDU^{3}–N^{C}.

isotherms are of type IV with an H2 hysteresis loop suggesting mesoporous materials. Pore size distributions reveal that the mesopores are highly ordered, but the pore volume and the specific surface area decrease slightly after such N-doping and further Pd immobilization (Table 1). This phenomenon is contrary to that of FDU^{3}–N^{H}. It has been reported that melamine molecules can be self-condensed to carbon nitride after appropriate thermal treatment and the resultant carbon nitride can be further decomposed at high temperature (>500 °C).[33,34] During our preparation, the composite of FDU^{3} and melamine was treated at 700 °C, and small part residue of carbon nitride could produce in the structure of FDU^{3}, which thus resulted in the decrease of the specific surface area and pore volume.

Figure 8 reveals that the SAXRD patterns of Pd@FDU^{3}–N^{C} show a significant decrease in the intensity of the lower-angle peak compared with FDU^{3}–N^{C} support, which can be attributed to the loading of the PdNPs that mainly formed

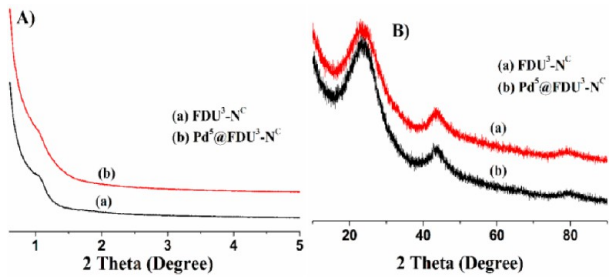

Figure 8. SAXRD (A) and WAXRD (B) patterns of FDU^{3}–N^{C} and Pd^{5}@FDU^{3}–N^{C}.

dx.doi.org/10.1021/cs400506q | ACS Catal. 2013, 3, 2440–2448

inside the channels of FDU^3−N^C. WAXRD patterns of FDU^3−N^C and Pd^5@FDU^3−N^C show the high-intensity of 002 and 100 diffractions belonging to graphitic carbon. Although the Pd loading content is as high as 5 wt %, the characteristic PdNPs peaks are not observed, suggesting that the small-sized PdNPs dispersed uniformly on the surface of the support. The TEM image reveals that FDU^3−N^C preserves an ordered hexagonal mesostructure and open pore networks without obvious pore blockage (Figure 9). Moreover, no obvious aggregations of

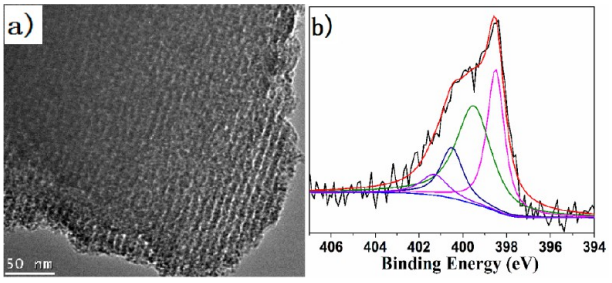

Figure 9. TEM image (a) and XPS N1s spectra (b) of FDU^3−N^C.

carbon nitride species outside the mesopore channels are observed even in a large domain, suggesting that the carbon nitrides are highly dispersed in the mesopore channels.

EA results are listed in Table 1, and they show a higher (7.8 wt %) nitrogen content of FDU^3−N^C than that of the data from XPS (6.6 wt %). The N1s XPS spectrum of FDU^3−N^C can be well fitted to four components.[30,35,36] The peak at 398.5 eV can be assigned to the pyridinic-type nitrogen. The predominant component at 399.5 eV is assigned to N atoms trigonally bonded to three sp2 carbons, further indicating the formation of carbon nitride. The peak at 400.5 eV is attributed to pyrrolic-type nitrogen. A comparatively weak peak at 401.3 eV can be associated with a classic graphitic-type quaternary nitrogen structure. In addition, the XPS results show that the surface oxygen content decreases from 8.5 to 5.3% because of the N-incorporation.

The TEM picture of Pd@FDU^3−N^C shows a few dark spherical spots which correspond to PdNPs that are clearly observed on the surface of the FDU^3−N^C support (Figure 10a). Accordingly, its HAADF-STEM image indicates that the PdNPs (white dots) are uniformly distributed and anchored along the surface of mesoporous carbons (Figure 10b); the PdNPs' average size is approximately 3.9 ± 0.8 nm (Figure 10c) and no agglomerations of PdNPs are observed in the HAADF-STEM image. The XPS measurements reveal a similar PdNP valence state with that of Pd^x@N^H-FDU^3 (Figure 10d).

Cyclohexanone is an important intermediate in the production of nylon 6 and nylon 66 in the chemical industry.[37−39] From the viewpoint of step economy and waste production, a "one-step" hydrogenation of phenol to cyclohexanone represents a more efficient and green process over the oxidation of cyclohexane and the "two-step" hydrogenation of phenol.[40] To achieve high efficiency in the "one-step" process, the development of a functional catalyst with the special property to control the selective hydrogenation is the key point because the cyclohexanone product is highly active towards further hydrogenation to give cyclohexanol. Recently, Han and co-workers reported that dual-supported Pd Lewis acid catalyst (Pd@C-AlCl$_3$) was a selective and efficient phenol hydrogenation catalyst through the AlCl$_3$ assisted activation of the phenyl ring and the prevention of further

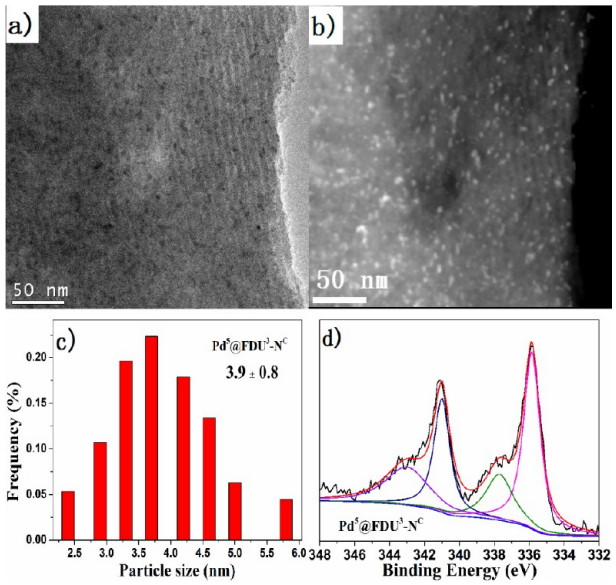

Figure 10. TEM (a) and HAADF-STEM (b) images, the particle size distribution (c), and the XPS Pd 3d spectra (d) of Pd^5@FDU^3−N^C.

hydrogenation.[41] Wang et al. described that PdNPs supported on a *mpg*-C_3N_4, prepared through hard-templating synthesis, are an efficient and selective catalyst in the hydrogenative transformation of phenol to cyclohexanone in water and under mild conditions.[19] Nevertheless, such Pd@mpg-C_3N_4 catalytic material has a low S_{BET} value (120 m^2/g), and a slight catalytic decrease was observed within four reaction runs. Additionally, the support without the doping of nitrogen was not used as a controllable support to investigate the effect of the N-doping. Considering that our series of Pd@FDU-N hybrid catalysts have high S_{BET} value (608−1487 m^2 g^{-1}), high nitrogen content (around 8.0 wt %), and tunable PdNPs size (1.2−4.4 nm), in this context, we selected a "one-step" hydrogenation of phenol to cyclohexanone as a reaction platform to investigate the effects of surface area, PdNPs' particle size, and mesopore structure of the present Pd@FDU-N catalysts, which demonstrated excellent catalytic performance and stability in such a clean transformation.

Initially, Pd$^{2.5}$@FDU^3−N^H was utilized as a typical catalyst to optimize the reaction conditions of the hydrogenation of phenol to cyclohexanone; the catalyst could show high catalytic conversion of phenol (85%) and excellent ketone selectivity (>98%) at low temperature (30 °C) and atmospheric H_2 pressure in 24 h (Entry 1, Supporting Information, Table S1). Increasing temperature could obviously shorten the reaction completion time (Entries 2−5, Supporting Information, Table S1), and a full conversion with >99% selectivity could be achieved at 100 °C within 2 h duration (Entry 6, Supporting Information, Table S1).

In principle, the supported nanoparticle size of a heterogeneous catalyst can have an important effect on the catalytic activity. Among these series of Pd@FDU-N catalysts, Pd^1@FDU^3−N^H, Pd$^{2.5}$@FDU^3−N^H, and Pd^5@FDU^3−N^H were prepared from the same N-doped FDU^3−N^H support and have almost the same structural properties (S_{BET} value and pore volume) except particle size. Therefore, it was very convenient to investigate the particle size effect of PdNPs by using these three different catalysts. As illustrated in Table 2, Pd^1@FDU^3−N^H with ultrasmall PdNP size (1.2 ± 0.3 nm) gave a 64%

dx.doi.org/10.1021/cs400506q | ACS Catal. 2013, 3, 2440−2448

Table 2. Hydrogenation of Phenol in Water with Different Catalysts[a]

entry	catalyst	conversion (%)	selectivity (%) C=O	selectivity (%) C−OH
1	Pd^{1}@FDU^{3}−N^{H}	69	>99	<1
2	$Pd^{2.5}$@FDU^{3}−N^{H}	45	>99	<1
3	Pd^{5}@FDU^{3}−N^{H}	22	>99	<1

[a]Reaction conditions: phenol (0.5 mmol), Pd (1.0 mol % relative to phenol), water (2.0 mL), H_2 (0.1 MPa), 100 °C, 1 h.

conversion of phenol within 1 h, $Pd^{2.5}$@FDU^{3}−N^{H} with middle PdNP size (2.3 ± 0.5 nm) afforded 45% hydrogenation conversion of the substrate, and only 22% conversion of phenol was obtained in the presence of Pd^{5}@FDU^{3}−N^{H} possessing the biggest PdNP size (3.3 ± 0.6 nm) under the same reaction conditions. Considering that particle size is the only difference among these catalysts (Table 1), it can be concluded that the supported nanoparticle size affects the catalytic performance significantly and that Pd^{1}@FDU^{3}−N^{H} with the ultrasmall PdNP size shows higher activity.

In addition, it has been reported that the Lewis additive or the basic functionalities of the support can influence the catalytic performance significantly.[19,41] Under our reaction conditions, commercial Pd@C with amorphous carbon as support only afforded 16% conversion of phenol and 83% selectivity of cyclohexanone (Table 3, entry 1). Pd^{5}@FDU^{3},

Table 3. Hydrogenation of Phenol in Water with Different Catalysts[a]

entry	catalysts	conversion (%)	selectivity (%) C=O	selectivity (%) C−OH
1[b]	Pd@C	16	83	17
2	Pd^{5}@FDU^{3}	23	95	5
3	Pd^{5}@FDU^{3}−N^{H}	80	>99	<1
4	Pd^{5}@FDU^{5}−N^{H}	78	>99	<1
5	Pd^{5}@FDU^{3}−N^{C}	57	>99	<1

[a]Reaction conditions: phenol (0.5 mmol), Pd (5 mol % relative to phenol), water (2.0 mL), H_2 (0.1 MPa), 100 °C, 1 h. [b]5%Pd@C was purchased from Alfa-Aesar.

which was prepared by immobilization of PdNPs on the pure OMCs, showed a slight catalytic enhancemen, possibly because the existence of the ordered mesoporous structure of Pd^{5}@FDU^{3} catalyst could partially promote the homogeneous distribution of PdNPs and facilitate mass transfer (Table 3, entry 2). Interestingly, the catalytic performance increased dramatically in the presence of Pd^{5}@FDU^{3}−N^{H}, with the N-functionalized OMC as the support (Table 3, entry 3), and quantitative conversion to the desired ketone product could be readily realized by prolonging the reaction time to 2 h (Supporting Information, Table S1, entry 8). This obvious catalytic increase could be attributed to the N-doping on the surface of the carbons because of the following two points: (1) the N-incorporation could stabilize the PdNPs during its liquid catalysis through electron donation from the N atom to the metallic PdNPs; (2) phenol substrate would interact with the N-incorporated groups on the surface of the mesoporous carbon support through the O−H···N interaction[19] and could thus adsorb a phenol molecule more effectively than the pure carbon. These two synergies could improve the catalytic activity and stability of present Pd@FDU-N catalyst.

Simultaneously, Pd^{5}@FDU^{3}−N^{H} and Pd^{5}@FDU^{5}−N^{H} have similar PdNP average particle size (3.3 ± 0.6 nm and 3.2 ± 0.6 nm, respectively) and identical N-doping nature, but different S_{BET} value, pore size, and volume (Table 1), and their obvious catalytic differences are not observed (Table 3, Entries 3−4), indicating that their S_{BET} value, pore size, and volume are high enough for the mass transfer and PdNP dispersion. However, the Pd^{5}@FDU^{3}−N^{C}, possessing a different N-doping support nature,[42,43] much lower S_{BET} value, and pore volume with that of Pd^{5}@FDU^{3}−N^{H}, demonstrated lower catalytic conversion of phenol compared with its counterpart (Pd^{5}@FDU^{3}−N^{H}).

To test the stability of this series of Pd@FDU-N catalysts under hydrothermal conditions, $Pd^{2.5}$@FDU^{3}−N^{H} was selected as the representative to investigate its recyclability in the hydrogenation of phenol in water. The recycling data in Figure 11 show that almost quantitative conversions of phenol to

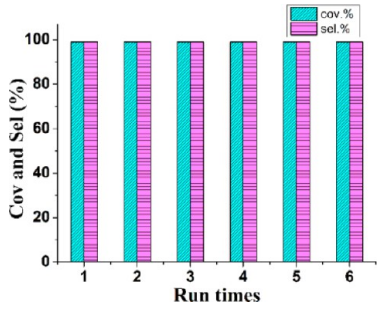

Figure 11. Recycling of the catalyst $Pd^{2.5}$@FDU^{3}−N^{H}. Reaction conditions: phenol (2 mmol), Pd (5 mol % relative to phenol), water (5.0 mL), H_2 (0.1 MPa), 100 °C, 2 h.

cyclohexanone are maintained within 6 reaction runs. Pd concentration of the liquid reaction solution was determined by ICP-AES to be less than 0.1 ppm, indicating that the leaching of Pd into the liquid phase is negligible. The separated $Pd^{2.5}$@FDU^{3}−N^{H} catalyst after the sixth reaction run was also examined by TEM, HAADF-STEM, and XPS. Compared with the fresh $Pd^{2.5}$@FDU^{3}−N^{H} (see Figure 5, 2a, 2b and 2c), TEM and HAADF-STEM images (Figure 12) of such recycled catalyst do not show any obvious change. The white dots, corresponding to PdNPs, are still mainly well-dispersed on the internal surface of the mesochanels, and the particle size distribution of the catalyst is 2.4 ± 0.4 nm, close to that of the fresh catalyst (2.3 ± 0.5 nm). The Pd 3d XPS data of the recycled $Pd^{2.5}$@FDU^{3}−N^{H} show that Pd^{0} is the main metal species on the surface of the catalyst, and the obvious change of Pd^{0} content is not detected. It further revealed that, in our case, the nitrogen-contained groups doped on the surface of the support were suitable for stabilizing highly dispersed Pd^{0} particles and preventing their aggregation and reoxidation.

3. CONCLUSION

The N-incorporation of ordered mesoporous FDU to produce FDU-N was easily realized by two different nitrogen sources; tunable and/or even ultrasmall particle size of PdNPs could be uniformly distributed on N-functionalized supports to afford a series of Pd@FDU-N catalysts, which provided an unique platform to investigate the influences of metal nanoparticle size, mesostructural properties, and N-functionalized support on catalytic performance, and the catalyst with ultrasmall (about 1.2 nm) PdNPs and N-doped support gave the best reaction activity and selectivity under mild conditions. It was

dx.doi.org/10.1021/cs400506q | ACS Catal. 2013, 3, 2440−2448

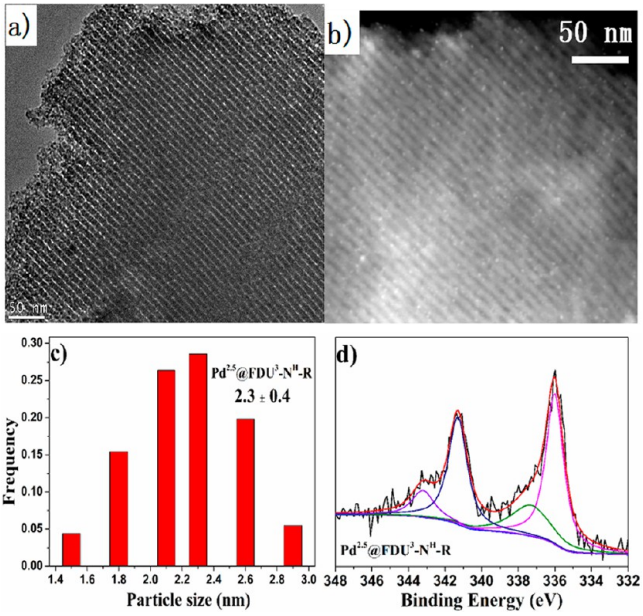

Figure 12. TEM (a) and HAADF-STEM (b) images, the particle size distribution (c), and the XPS Pd 3d spectra (d) of recycled $Pd^{2.5}$@ FDU^3-N^H after 6 runs.

experimentally revealed that the doped nitrogen could not only disperse and stabilize the small-sized PdNPs but also enhance the catalytic hydrogenation activity and selectivity through weak interaction with the phenol molecule. In addition, the present catalyst showed good stability and could be used for 6 times without loss of its product yields.

4. EXPERIMENTAL SECTION

4.1. Materials. All chemicals were purchased from commercial sources and were used without further purification. The OMC FDU-15 was purchased from unicarbonshanghai. Two types of FDU-15 were utilized in this work, one had a 600 $m^2\ g^1$ BET surface area and a 3 nm average pore diameter and another possessed a 1100 $m^2\ g^{-1}$ BET surface area and with a pore diameter of 5.1 nm. These two FDU-15 materials were nominated for FDU^3 and FDU^5, respectively.

4.2. N-Functionalization of FDU-15 with NH_3 Gas via Thermal Ammonolysis. Nitridation was performed in a plug-flow fixed-bed quartz reactor with an inner diameter of 5 mm placed vertically inside the tubular furnace. Typically, 200−300 mg of FDU-15 was loaded in the reactor, and the furnace was heated to 100 °C at a ramp rate of 1 °C/min under a 100 mL/min flow of nitrogen atmosphere. Subsequently, the reactor was further heated up under pure ammonia gas flow with a speed of 300 mL/min and held for 10 h at the desired temperature (700 °C). After that, the furnace was cooled to 100 °C and the gas flow was changed to 100 mL/min of nitrogen to further cool the reactor to room temperature (RT), yielding the resultant NOMC samples, which were accordingly designated as FDU^3-N^H or FDU^5-N^H.

4.3. N-Functionalization of FDU-15 with Melamine via Heat Treatment. Nitridation was carried out in the same reactor. In general, FDU-15 (600 mg) and melamine (600 mg) were added into an 100 mL round-bottom flask with 20 mL of ethanol, and the resultant mixture was heated to 80 °C to volatilize the solvent under stirring. Finally, the solid mixture was loaded in the high temperature reactor, and the furnace was heated up to 700 °C at a ramp rate of 3 °C/min and further held for 2 h, then the reactor was cooled to RT under the above-mentioned conditions. The obtained NOMC material was named FDU^3-N^C.

4.4. Immobilization of Pd Nanoparticles. An aqueous solution of H_2PdCl_4 was initially prepared by mixing 0.34 g of $PdCl_2$ into 20 mL of 10% v/v HCl aqueous solution by stirring at RT until the salt was homogeneously dissolved. Then, a certain amount of the prepared mesoporous FDU^3-N^H, FDU^5-N^H, and FDU^3-N^C powder was impregnated with the H_2PdCl_4 solution and stirred for 5 h at RT. Then excess $NaBH_4$ aqueous solution was slowly added to such a suspension mixture under ice bath conditions. Finally, the corresponding supported PdNPs were separated by centrifugation, washed sequentially with distilled water and absolute ethanol several times, and dried at 80 °C overnight in a vacuum oven to give the corresponding PdNP catalysts (Pd^X@FDU-N^Y), wherein X represents the Pd loading percent and Y stands for H or C.

4.5. Pd^X@FDU-N^Y Catalyzed Hydrogenation of Phenol. Catalytic tests were conducted in a 50 mL Schlenk glass tube with a magnetic bar; heterogeneous Pd catalyst, phenol, and water were introduced into the glass tube, and then it was vacuumed and purged with H_2 three times before it was finally pressurized with 1.0 atm of H_2 gas. Subsequently, the reaction mixture was stirred at a given temperature. After cooling to RT, excess H_2 was carefully released, and the internal standard (toluene) was added. The resultant product mixtures were analyzed by an Agilent gas chromatograph.

4.6. Instruments. Pd content and immobilization yield were obtained by ICP-AES analysis using a Perkin-Elmer OPTIMA 3300 DV (Norwalk, CT, U.S.A.). Powder X-ray diffraction (XRD) measurements were performed on an X'Pert Pro multipurpose diffractometer (PANalytical, Inc.) with Ni-filtered CuKα radiation (0.15046 nm) at RT from 10.0° to 80.0° (wide angle) and 0.6° to 5° (small angle). The nitrogen adsorption and desorption isotherms at −196 °C were recorded on an Autosorb-iQ analyzer (Quantachrome Instruments, Boynton Beach, FL), and samples were degassed for 4 h at 300 °C before analysis. The specific surface areas were calculated via the BET method in the relative pressure range of 0.05−0.3. The single-point pore volume was calculated from the adsorption isotherm at a relative pressure of 0.990; pore size distributions were calculated using adsorption branches of nitrogen adsorption−desorption isotherms by the BJH method. TEM and HRTEM experiments were conducted in a JEM-2010 TEM with an accelerating voltage of 200 kV. XPS analyses of the catalysts were performed on a Thermo Fisher Scientific K-Alpha spectrometer.

■ ASSOCIATED CONTENT

Supporting Information

Figure S1 (XPS spectra of Pd@FDU-N^H), and Table S1. This material is available free of charge via the Internet at http://pubs.acs.org.

■ AUTHOR INFORMATION

Corresponding Authors

*E-mail: cgxia@licp.cas.cn (C.X.).
*E-mail: fuweili@licp.cas.cn (F.L.).

Notes

The authors declare no competing financial interest.

■ ACKNOWLEDGMENTS

This work was supported by the Chinese Academy of Sciences and the National Natural Science Foundation of China (21002106, 21133011, and 21373246).

■ REFERENCES

(1) Kibata, T.; Mitsudome, T.; Mizugaki, T.; Jitsukawa, K.; Kaneda, K. *Chem. Commun.* **2013**, *49*, 167.
(2) Tyo, E. C.; Yin, C.; Di Vece, M.; Qian, Q.; Kwon, G.; Lee, S.; Lee, B.; DeBartolo, J. E.; Seifert, S.; Winans, R. E.; Si, R.; Ricks, B.; Goergen, S.; Rutter, M.; Zugic, B.; Flytzani-Stephanopoulos, M.; Wang, Z. W.; Palmer, R. E.; Neurock, M.; Vajda, S. *ACS Catal.* **2012**, *2*, 2409.
(3) Qiao, B.; Wang, A.; Yang, X.; Allard, L. F.; Jiang, Z.; Cui, Y.; Liu, J.; Li, J.; Zhang, T. *Nat. Chem.* **2011**, *3*, 634.
(4) Vajda, S.; Pellin, M. J.; Greeley, J. P.; Marshall, C. L.; Curtiss, L. A.; Ballentine, G. A.; Elam, J. W.; Catillon-Mucherie, S.; Redfern, P. C.; Mehmood, F.; Zapol, P. *Nat. Mater.* **2009**, *8*, 213.
(5) Lu, J.; Fu, B.; Kung, M. C.; Xiao, G.; Elam, J. W.; Kung, H. H.; Stair, P. C. *Science* **2012**, *335*, 1205.
(6) Prieto, G.; Zečević, J.; Friedrich, H.; de Jong, K. P.; de Jongh, P. E. *Nat. Mater.* **2013**, *12*, 34.
(7) Oliver-Meseguer, J.; Cabrero-Antonino, J. R.; Domínguez, I.; Leyva-Pérez, A.; Corma, A. *Science* **2012**, *338*, 1452.
(8) Xin, H. L.; Mundy, J. A.; Liu, Z.; Cabezas, R.; Hovden, R.; Kourkoutis, L. F.; Zhang, J.; Subramanian, N. P.; Makharia, R.; Wagner, F. T.; Muller, D. A. *Nano Lett.* **2011**, *12*, 490.
(9) Ott, L. S.; Finke, R. G. *Coord. Chem. Rev.* **2007**, *251*, 1075.
(10) Li, X.-H.; Antonietti, M. *Chem. Soc. Rev.* **2013**, *42*, 6593−6604.
(11) Datta, K. K. R.; Balasubramanian, V. V.; Ariga, K.; Mori, T.; Vinu, A. *Chem.—Eur. J.* **2011**, *17*, 3390.
(12) Wu, Z.; Lv, Y.; Xia, Y.; Webley, P. A.; Zhao, D. *J. Am. Chem. Soc.* **2011**, *134*, 2236.
(13) Li, X.-H.; Wang, X.; Antonietti, M. *Chem. Sci.* **2012**, *3*, 2170.
(14) Gong, Y.; Zhang, P.; Xu, X.; Li, Y.; Li, H.; Wang, Y. *J. Catal.* **2013**, *297*, 272.
(15) Xu, X.; Li, Y.; Gong, Y.; Zhang, P.; Li, H.; Wang, Y. *J. Am. Chem. Soc.* **2012**, *134*, 16987.
(16) Li, Y.; Xu, X.; Zhang, P.; Yutong, G.; Li, H.; Wang, Y. *RSC Adv.* **2013**, *3*, 10973.
(17) Zhang, P.; Gong, Y.; Li, H.; Chen, Z.; Wang, Y. *Nat. Commun.* **2013**, *4*, 1593.
(18) Datta, K. K. R.; Reddy, B. V. S.; Ariga, K.; Vinu, A. *Angew. Chem., Int. Ed.* **2010**, *49*, 5961.
(19) Wang, Y.; Yao, J.; Li, H.; Su, D.; Antonietti, M. *J. Am. Chem. Soc.* **2011**, *133*, 2362.
(20) Yang, S.; Zhi, L.; Tang, K.; Feng, X.; Maier, J.; Müllen, K. *Adv. Funct. Mater.* **2012**, *22*, 3634.
(21) Wang, X.; Lee, J. S.; Zhu, Q.; Liu, J.; Wang, Y.; Dai, S. *Chem. Mater.* **2010**, *22*, 2178.
(22) Mahurin, S. M.; Lee, J. S.; Wang, X.; Dai, S. *J. Membr. Sci.* **2011**, *368*, 41.
(23) Wu, Z.; Webley, P. A.; Zhao, D. *J. Mater. Chem.* **2012**, *22*, 11379.
(24) Li, Z.; Liu, J.; Huang, Z.; Yang, Y.; Xia, C.; Li, F. *ACS Catal.* **2013**, *3*, 839.
(25) Datta, K. K. R.; Balasubramanian, V. V.; Ariga, K.; Mori, T.; Vinu, AT. *Chem.—Eur. J.* **2011**, *17*, 3390.
(26) Boehm, H. P.; Mair, G.; Stoehr, T.; De Rincón, A. R.; Tereczki, B. *Fuel* **1984**, *63*, 1061.
(27) Radkevich, V. Z.; Senko, T. L.; Wilson, K.; Grishenko, L. M.; Zaderko, A. N.; Diyuk, V. Y. *Appl. Catal., A* **2008**, *335*, 241.
(28) Stöhr, B.; Boehm, H. P.; Schlögl, R. *Carbon* **1991**, *29*, 707.
(29) Kelemen, S. R.; Afeworki, M.; Gorbaty, M. L.; Kwiatek, P. J.; Solum, M. S.; Hu, J. Z.; Pugmire, R. J. *Energy Fuels* **2002**, *16*, 1507.
(30) Li, X.; Wang, H.; Robinson, J. T.; Sanchez, H.; Diankov, G.; Dai, H. *J. Am. Chem. Soc.* **2009**, *131*, 15939.
(31) Pietrzak, R. *Fuel* **2009**, *88*, 1871.
(32) Wei, D.; Liu, Y.; Wang, Y.; Zhang, H.; Huang, L.; Yu, G. *Nano Lett.* **2009**, *9*, 1752.
(33) Zhao, Y.; Liu, Z.; Chu, W.; Song, L.; Zhang, Z.; Yu, D.; Tian, Y.; Xie, S.; Sun, L. *Adv. Mater.* **2008**, *20*, 1777.
(34) Yan, S. C.; Li, Z. S.; Zou, Z. G. *Langmuir* **2009**, *25*, 10397.
(35) Vinu, A.; Ariga, K.; Mori, T.; Nakanishi, T.; Hishita, S.; Golberg, D.; Bando, Y. *Adv. Mater.* **2005**, *17*, 1648.
(36) Lezanska, M.; Pietrzyk, P.; Sojka, Z. *J. Phys Chem. C* **2009**, *114*, 1208.
(37) Barrett, E. P.; Joyner, L. G.; Halenda, P. P. *J. Am. Chem. Soc.* **1951**, *73*, 373.
(38) Chen, Y. Z.; Liaw, C. W.; Lee, L. I. *Appl. Catal., A* **1999**, *177*, 1.
(39) Mahata, N.; Vishwanathan, V. *J. Catal.* **2000**, *196*, 262.
(40) Chatterjee, M.; Kawanami, H.; Sato, M.; Chatterjee, A.; Yokoyama, T.; Suzuki, T. *Adv. Synth. Catal.* **2009**, *351*, 1912.
(41) Liu, H.; Jiang, T.; Han, B.; Liang, S.; Zhou, Y. *Science* **2009**, *326*, 1250.
(42) Casanovas, J.; Ricart, J. M.; Rubio, J.; Illas, F.; Jiménez-Mateos, J. M. *J. Am. Chem. Soc.* **1996**, *118*, 8071.
(43) Wang, H.; Maiyalagan, T.; Wang, X. *ACS Catal.* **2012**, *2*, 781.